A possible mechanism for ENSO turnabouts

Bin Wang*, Renguang Wu, Roger Lukas, and Soon-Il An*

School of Ocean and Earth Science and Technology, University of Hawaii,

Honolulu, HI 96822, USA

Submitted to J. Climate

July 8, 1999

Corresponding author's address: Dr. Bin Wang, Department of Meteorology and International Pacific Research Center, University of Hawaii, 2525 Correa Road, Honolulu, Hawaii 96822. E-mail: bwang@soest.hawaii.edu

* Member of the International Pacific Research Center (IPRC). IPRC is sponsored in part by the Frontier Research System for Global Change.

Abstract

The reversal of warming or cooling trends of ENSO cycles occurs most frequently toward the end of the calendar year. A possible mechanism is advanced based on observational evidence and model results. Prior to the peaks of major warm (cold) episodes, an anomalous surface anticyclone (cyclone) establishes rapidly over the Philippine Sea. To the south of the anticyclone (cyclone), anomalous easterlies (westerlies) prevail in the equatorial western Pacific and, by forcing oceanic equatorial upwelling (downwelling) Kelvin waves, provides a negative feedback to the eastern Pacific warming (cooling). In the western North Pacific, the coherent variations in the surface winds and SST suggest a local positive feedback between the Philippine Sea anomalous anticyclone (cyclone) and negative (positive) SST anomalies. This positive feedback plays critical roles in intensification and maintenance of the wind and SST anomalies in the Philippine Sea. This positive feedback also depends on the existence of mean northeasterly trades and the central Pacific warming during the *boreal cold season*. Therefore, the proposed negative feedback favors the turnabouts of ENSO cycles in boreal winter.

This hypothesis was tested using a modified Cane-Zebiak coupled model in which the original atmosphere model was replaced by an empirical atmosphere model derived from the singular value decomposition of observations. The empirical atmospheric model contains significant seasonally-dependent wind anomalies in the western Pacific. The model results indicate that the annual variation of the anomalous western Pacific winds favors reversal of the warming and cooling trends toward the end of the calendar year. Without this process, the coupled model fails to reproduce the preferred occurrence of the cold peaks in boreal winter.

1. Introduction

The unprecedented 1997-98 El Niño reached its peak in November-December 1997. The reversal of warming trends toward the end of the calendar year is typical. Figure 1 shows monthly mean sea surface temperature (SST) anomalies averaged in the key region of the Pacific warming--NINO3.4 (5ºS-5ºN, 120ºW-170ºW). During the period of 1957-1998, the magnitudes of the NINO3.4 SST anomalies exceeded 1.5 times the standard deviation in seven warm (57/58, 65, 72, 82/83, 86/87, 91/92, 97/98) and five cold (70/71, 73/74, 75/76, 84/85, and 88/89) episodes. Figure 2 displays the monthly mean NINO3.4 SST anomalies for these warmest and coldest episodes except for the 1986-87 event. In all these major episodes, the NINO3.4 SST anomalies reached 1.5 times the standard deviation by November of the ENSO (El Niño or La Niña) development year. Furthermore, the intense warming or cooling is followed by a reversal of the warming or cooling trends from November to the following January. This indicates a strong tendency of ENSO turnabout (reversal of warming or cooling trends) occurring in boreal winter. Although the evolution of ENSO and its time of transition from cold to warm states has experienced an apparent interdecadal change in the late 1970's (Wang 1995a), the phase-lock of the ENSO turnabout remains robust. During the exceptional 1986-87 event, the warming developed in 1986; however, the NINO3.4 SST anomalies failed to reach 1.5 times the standard deviation by November of that same year. The reversal of the warming trend was delayed to the fall of 1987. In this paper, we will focus on the common features of the six warmest and five coldest events shown in Fig. 2, while discussing the 1986-87 event as a special case in the last section.

The phase-lock of ENSO events to the annual cycle is an essential feature of the ENSO

dynamics (Philander and Rasmusson 1985). However, the physical processes determining this phase-lock are not yet well understood. The widely accepted delayed oscillator theory (Schopf and Suarez 1988, Suarez and Schopf 1988, Battisti and Hirst 1989, Cane et al. 1990) implicates oceanic Rossby wave reflection at the western boundary as a key process for the ENSO turnabout. Although the efficiency of the western boundary as a wave reflector was questioned (e.g., Li and Clarke 1994, Kessler and McPhaden 1995), the delayed oscillator theory provides a plausible explanation for a sustained oscillation of the coupled system. It explains why the oceanic thermocline adjustment lags wind variations and how the phase-lagged adjustment provides a negative feedback to reverse the trends of SST variation; but it does not explain why the turnabout should prefer boreal winter. It has been proposed that the seasonally varying strength of the coupled ocean-atmosphere instability may account for the ENSO phase-lock to the annual cycle (Tziperman et al. 1998, Wang and Fang 1996). However, the models used to demonstrate this mechanism do not necessarily reproduce the observed phase-lock of the peak cold events to boreal winter (as will be shown in section 6). In addition, the degree of phase-lock in these models decreases with increasing model oscillation period. While the oceanic wave dynamics in the presence of the annual cycle of the mean states can provide a negative feedback, it is not the only mechanism for ENSO turnabout.

During the ENSO turnabouts, wind anomalies are prominent in the western Pacific: a rise of sea-level pressure over the western North and South Pacific (Wang 1995b, Harrison and Larkin 1996) is accompanied by a strengthening of easterlies over the equatorial western Pacific (Rasmusson and Carpenter 1982, Deser and Wallace 1989). Previous studies have speculated that these anomalous winds observed in the equatorial western Pacific and Philippine Sea may contribute to the reversal of the warming (Weisburg and Wang 1997, Wang et al. 1999a).

However, the physical mechanism has not been clarified. Weisburg and Wang (1997) argued that the western Pacific easterly anomalies are associated with local high pressure that is induced by the sea surface cooling due to westward propagation of oceanic upwelling Rossby waves excited in the central Pacific. This speculation essentially ties these easterly anomalies to a by-product of the delayed oscillator mechanism. Since the thermocline in the off-equatorial western Pacific is deep (about 150 m), it is questionable whether the upwelling waves can cause sufficient SST cooling. In fact, in the Zebiak and Cane (1987) model, the western Pacific cooling is extremely weak, albeit the model develops strong upwelling Rossby waves and the model ENSO relies on the vertical temperature advection. Furthermore, the previous observational analyses have shown that the positive pressure anomalies in the western North Pacific lag, rather than lead, the warm peak (Wang 1995b, Harrison and Larkin 1996). The easterly anomalies over the equatorial western Pacific also tend to follow the peak of the eastern-central Pacific warming (Mayor and Weisburg 1998). Thus, the anomalous easterly winds cannot be an *origin* of the turnabout for a warm event. Finally, in order to reverse the warming trend, the easterly anomalies in the equatorial western Pacific must persist. Given the chaotic nature of the atmospheric motion, it is not obvious how the western Pacific easterly anomalies (that blow against the forcing induced by the central Pacific warming) can last and provide a continuing negative feedback to eventually turn around ENSO cycles. In particular, no explanation is given as to why the ENSO turnabout most frequently occurs in boreal winter.

The present paper proposes a possible mechanism that favors the ENSO turnabout in boreal winter. This new mechanism works for major warm or cold episodes and is independent of the propagation and reflection of the oceanic Rossby waves. The preferred winter turnabout can be caused by an atmospheric teleconnection between the central Pacific warming (cooling)

and the East Asian winter monsoon (Wang et al. 1999b). To elaborate on this mechanism, we will specifically address the following issues:

(1) What is the phase relationship between the change of the western Pacific winds and the ENSO turnabouts? How does the equatorial ocean respond to the changes of winds in the western Pacific?

(2) How do the wind anomalies in the western Pacific develop and how are they maintained? Why do they tend to occur in boreal winter?

(3) What roles do the western Pacific wind anomalies play in a coupled ocean-atmospheric model?

This paper consists of an observational analysis that addresses the first two questions (sections 2 and 3) and a modeling study that addresses the third question (section 4). In section 2, we show evidence that the *sudden change* of the sea level pressure over the Philippine Sea and the accompanying sudden establishment of the equatorial zonal wind anomalies north of New Guinea *lead* the warm or cold peaks in the equatorial central Pacific. We also show evidence of the equatorial oceanic Kelvin waves that are excited by the *sudden change* of the winds in the western Pacific. These Kelvin waves induce thermocline displacement that can potentially contribute to the demise of the eastern-central Pacific warming or cooling. In section 3, we show evidence that the sudden development and maintenance of the western Pacific wind anomalies depend on a local positive feedback between the Philippine Sea anticyclone (cyclone) and negative (positive) SST anomalies. This positive feedback depends critically on mean surface winds in boreal winter. This leads to a seasonally dependent mechanism for the ENSO turnabouts. To test this hypothesis, we use a modified Zebiak and Cane (1987) model and perform a series of numerical experiments (section 4). The results of the numerical experiments

demonstrate the importance of the western Pacific wind anomalies in the phase lock of the ENSO turnabout to the annual cycle. The last section discusses the future work that is needed for further verification of the hypothesis developed in this work.

2. Philippine Sea wind anomalies and their impacts on the equatorial ocean

a. Sudden establishment of the Philippine Sea wind anomalies prior to ENSO turnabouts

We discovered that *prior to* the peaks of the warm (cold) episodes, a large-scale, anomalous high (low) pressure establishes rapidly in the lower troposphere over the Philippine Sea. For convenience of comparison, we plot in Fig. 2 the NINO 3.4 SST anomalies along with the sea level pressure anomalies in the Philippine Sea (120-150ºE, 10-20ºN) and the zonal wind anomalies averaged over the equatorial western Pacific (120-150ºE, 4°S-4ºN). A sharp increase in sea level pressure over the Philippine Sea precedes the warm peak by about one or two months (Fig. 2a). In harmony with this pressure tendency, a strong anomalous anticyclone occurs over the Philippine Sea accompanied by enhanced easterlies north of the New Guinea in the equatorial western Pacific. In sharp contrast, two to three months prior to the peak of cold events, anomalous low pressure and a cyclone are suddenly initiated over the Philippine Sea with westerly anomalies prevailing in the equatorial western Pacific (Fig. 2b). The striking similarities within the group of the warm or cold episodes and the contrast between the two groups warrant a statistically significant composite for each group.

Figures 3a and 3b display a composite evolution for the six warmest and five coldest events shown in Fig. 2, respectively. From –2 to –1 month (the time lag here is defined with respect to the time of the warm or cold peak), there is a prominent increase in the Philippine Sea

pressure and the strength of the easterlies over the equatorial western Pacific. Likewise, a pronounced decrease in the Philippine Sea pressure and the equatorial western Pacific easterlies occurs from –3 to –2 month before the cold peak.

To show the spatial structure of the rapid changes, we display in Fig. 4 the tendency of the monthly mean 1000hPa winds at –1 month (one month prior to the warm peaks) for the six warmest episodes. There is a notable feature common to all major warm episodes, i.e., sudden enhancement of the anticyclone in the Philippine Sea and the easterlies north of New Guinea, which confirms the finding shown in Fig. 2a.

To better display this common feature, we present in Fig. 5a a composite tendency map for the sea level pressure and 1000hPa winds for the warmest events shown in Fig. 4. The composite is made by subtracting the sea level pressure and 1000 hPa winds at the -2 month from those at the –1 month. Thus, the composite tendency field leads the composite warm peak by one month. Similarly, Fig. 5b presents a composite tendency map of cold events at –2 month (two months before the cold peak). We take two months before the cold peak because the sharp decreases of pressure and easterlies occur from –3 to –2 month in the composite coldest events (Fig. 3b). Statistical significance of the composite wind tendencies between the warm and cold composites is tested using t- and F-tests. The wind anomalies over the Philippine Sea and north of New Guinea are significant at the 95% confidence level. Prior to the warm (cold) peak, anticyclonic (cyclonic) wind anomalies over the Philippine Sea and associated easterly (westerly) wind anomalies in the equatorial western Pacific develop abruptly. Though the timing of the maximum tendency for each event varies, the changes from –2 to –1 (-3 to –2) month with reference to the warm (cold) peaks are sufficiently common to warrant a statistically significant tendency as shown in Fig. 5. Although the wind anomalies in the equatorial central Pacific

associated with the ENSO warming (cooling) are much more intense than the wind anomalies north of New Guinea, their tendencies are weak and statistically insignificant, because these wind anomalies evolve slowly, reflecting a slow coupled ocean-atmospheric mode. This suggests that the rapid establishment of the tropical wind anomalies over the Philippine Sea differs from the evolution of the slow coupled mode, and that it is not a direct response to the equatorial central Pacific SST anomalies.

Although the rapid development of the western North Pacific (WNP) wind anomalies leads the peak warm (cold), the extrema of the Philippine Sea surface pressure and the equatorial western Pacific surface zonal wind anomalies tend to lag the corresponding extrema of NINO 3.4 SST anomalies (Figs. 2 and 3). This fact explains why the previous lag-correlation (Wang 1995b) or empirical orthogonal function analyses (Mayor and Weisburg 1998) failed to detect the phase lead of the *sudden change* to the warm (cold) peak. Obviously, the results of the lag-correlation and EOF analyses were dominated by the large variances associated with the extreme values of the fields.

b. Forced ocean response to the sudden changes in the western Pacific wind anomalies

The sudden emergence of the easterly (westerly) anomalies over the western equatorial Pacific may generate equatorial upwelling (downwelling) Kelvin waves. The forced equatorial Kelvin waves have been well documented in the previous observations (e.g., Knox and Halpern 1982, Eriksen et al. 1983, Lukas et al. 1984). To examine possible excitation of the *forced* Kelvin waves by the wind anomalies associated with the Philippine Sea anticyclone (cyclone) during the mature phases of warm (cold) events, we used the data derived from the NCEP Ocean Data Assimilation System (Ji et al. 1995).

Figures 6 and 7 show local rates of change of the subsurface temperature (referred to as temperature tendency hereafter) in a vertical section along the equator. The tendencies of the subsurface temperature result primarily from vertical displacement of the thermocline that is mainly caused by the passage of the equatorial Kelvin waves.

In December 1991, one month before the peak of the 1991/92 warm event, a sudden increase of easterlies over the equatorial western Pacific (Fig. 2a, Fig. 4) appears to induce upwelling that elevated the thermocline, causing temperature decreases at its mean depth (Fig. 6b). The region of decreased temperature (signals of upwelling or cold Kelvin waves) then migrated eastward at a speed of about 40-50 longitudes per month along the thermocline. The enhancement of anomalous easterlies in February 1992 (Fig. 2a) triggered a second set of cold Kelvin waves that propagated all the way to the equatorial eastern Pacific (Fig. 6b). The consecutive eastward passage of upwelling Kelvin waves contributed to the recovery of the thermocline slope in the eastern Pacific and the decay of the warming.

Prior to the peak of the 1982-83 event, from October to December 1982, the Philippine Sea anticyclone and the equatorial easterly anomalies continuously built up (Fig. 2a). A pronounced increase in the equatorial easterlies is seen in the tendency map of December 1982 with a monthly mean anomalous wind speed exceeding 5 m/s (Fig. 4). The easterly anomalies induced a sharp rise of the thermocline in December 1982, as signified by a decrease of thermocline temperature by more than six degrees (Fig. 6a). The rising thermocline reaches the eastern boundary about two months later. As a result, the flattened thermocline starts to recover its slope. The 1982-83 event differs from the 91-92 event in that the equatorial easterly anomalies in the western Pacific persisted without significant month-to-month fluctuations (Fig. 2a). This is reflected in the corresponding equatorial ocean response.

Conversely, prior to the peak of the 1988-89 cold event in October 1988, the abrupt enhancement of westerlies in the equatorial western Pacific (Fig. 2b) deepened the thermocline, triggering a downwelling or warm Kelvin wave that propagated eastward along the tilted thermocline (Fig. 7b). The enhanced westerlies in December 1988 (Fig. 2b) sent another set of warm Kelvin waves to the eastern Pacific. A similar sequence of downwelling Kelvin wave episodes occurred in the 1984-85 cold event. Corresponding to the enhanced westerlies in the western equatorial Pacific in October 1984, December 1984-January 1985, and March 1985 (Fig. 2b), three sets of downwelling Kelvin waves were generated in the equatorial western Pacific (Fig. 7a). Although the temporal resolution of the data is inadequate for resolving subseasonal fluctuations, the timing of the thermocline deepening and the enhancement of the equatorial westerlies appear to be in good agreement.

The consecutive generation and passage of upwelling (downwelling) Kelvin waves into the eastern Pacific can effectively erode equatorial surface cooling (warming) as they journey to the east. Because the sudden change of zonal winds in the equatorial western Pacific leads the warm (cold) peak of the ENSO cycle, it is possible that these wind anomalies play an active role in initial reversal of the warming (cooling) trend. The equatorial thermocline adjustment that is critical to ENSO turnabouts appears to involve multiple time scales. The fast time scale is associated with the eastward propagation of Kelvin waves forced by the month-to-month wind fluctuations or intraseasonal oscillations in the western Pacific. The variation on the slow time scale is seen from the gradual recovery of the thermocline slope after the warm peak (Figs. 6 and 7). The latter also manifests itself as a slow eastward propagation of negative upper ocean heat content anomalies (Chao and Philander 1993), which is in tandem with the slow eastward movement of the central Pacific easterly anomalies and suppressed convection. This slow

variation reflects a coupled atmosphere-ocean mode (Philander et al. 1984, Hirst 1986).

The fast Kelvin waves and the slowly coupled mode are likely interactive. A rise of the thermocline in the eastern Pacific due to the arrival of a forced upwelling Kelvin wave may initially offset local warming, which would in turn intensify SST gradients and restore equatorial easterlies, thereby inducing a slow thermocline shoaling and SST decrease in the eastern Pacific. Consecutive generation and passage of forced Kelvin waves may stimulate slow eastward migration of the heat content through the "fetch extension" mechanism (Kessler and McPhaden 1995) or the zonal advection process (Lukas et al. 1984, Picaut et al. 1996). The simulation of the 1997-98 warm event indicates that the upwelling Kelvin waves generated by the easterly anomalies in the western Pacific contributed to the shoaling of the thermocline and the demise of the warming (McPhaden and Yu 1999).

The wind stress curl associated with the Philippine Sea wind anomalies directly displaces the thermocline vertically via Ekman pumping (Wang et al. 1999b). The sudden establishment of the Philippine Sea anticyclone may force downwelling Rossby waves that, upon reflection from the western boundary, may induce downwelling Kelvin waves which oppose the vertical displacement of the thermocline directly forced by the equatorial easterly anomalies south of the Philippine Sea anticyclone. However, a phase delay between the reflected and locally forced Kelvin waves is anticipated, so their effects are not expected to cancel each other. However, the relative contributions of these waves can not be assessed unless a coupled model is used. In section 5, we will use a coupled model to determine the impacts of the western Pacific wind anomalies on ENSO turnabouts.

3. Seasonal dependence of the ENSO turnabouts

a. Causes of the development and maintenance of the WNP wind and SST anomalies

To reach the opposite phase of ENSO, the reversed trend must endure. Figure 2a indicates that during and after the mature warm phase, the Philippine Sea anomalous anticyclone and associated equatorial easterly anomalies indeed persist for two to three seasons following their rapid establishment, although significant month-to-month fluctuations exist in their intensities. After the peak of each major cold episode, the Philippine Sea cyclonic anomalies and associated equatorial westerly anomalies also persisted for at least four months (Fig. 2b). Because the atmosphere has no long-term memory, a question that must be addressed is how the Philippine Sea and associated equatorial wind anomalies are maintained.

To understand how the Philippine Sea wind anomalies persist, we need to examine the evolution of the wind and SST anomalies. Figure 8 presents the evolution of composite SST and 1000 hPa wind anomalies during the reversal of the warming trend from –3 month to +4 month (the minus and plus signs indicate before and after the warm peak, respectively). From –2 to –1 month, the anomalous winds over the Philippine Sea suddenly change from cyclonic to anticyclonic. In the front of the anticyclone, cooling starts to strengthen in the vicinity of (160ºE, 10ºN). The anomalous anticyclone and enhanced negative SST anomalies (less than -0.4ºC) persist from –1 to +4 month. Both wind and SST anomalies migrate and expand slowly eastward.

To further display the coherent variation between the atmosphere and ocean, we present evolution of the composite SST, surface winds, and 1000 hPa pressure anomalies for the six warmest episodes across the North Pacific (Fig. 9). The SST and 1000 hPa winds were averaged between 5°N and 15°N, while the pressure anomalies were averaged between 10ºN and 20ºN.

The latitudes chosen for pressure are located slightly north of the latitudes for SST anomalies because the atmospheric Rossby wave response is located to the north and west of the SST anomalies. Fig. 9a indicates that from –2 to –1 month the WNP cooling intensifies between 140ºE and the dateline; meanwhile, an accompanying warming occurs over the South China Sea and Philippine Islands between 100ºE and 130ºE. Note that the cooling (warming) coincides with northerly (southerly) anomalies. Concurrent with the enhancement of the cooling, the sea level pressure between 140ºE and the dateline rises rapidly from –2 to –1 month (Fig. 9b). Both the SST and the sea level pressure anomalies show a coherent slow eastward expansion.

The coherent variations in the surface winds (pressure) and SST shown in Figs. 8 and 9 suggest a coupled nature of the surface winds and SST in the WNP. More importantly, Figs. 8 and 9 indicate that the anomalous anticyclone center is located about 20 degree longitude west of the maximum cooling (Fig. 9). Using the COLA atmospheric general circulation model (Kirtman and DeWitt 1997) and the University of Hawaii intermediate atmospheric model (Wang and Li 1993, Fu and Wang 1999), we have shown that the anticyclone results primarily from a Rossby wave response to the local cooling (Wang et al. 1999a). From an oceanographic point of view, the anomalous anticyclonic winds superposed on mean northeasterly trades increase the total wind speed, thus enhancing the evaporation and entrainment to the east of the anticyclone. This in turn favors sea surface cooling in front of the anticyclone. Therefore, the phase shift between the anticyclone and sea surface cooling implies a local positive feedback that can amplify and sustain the Philippine Sea anticyclonic wind and the negative SST anomalies in the presence of the boreal winter mean circulation. Consideration of the cloudiness anomalies associated with the anticyclone may reduce the phase shift between the anticyclone and cold SST anomalies, but would not destroy this positive feedback. Thus, the positive feedback between the anticyclone

and sea surface cooling through evaporation and entrainment processes provides a mechanism for the development and maintenance of the western Pacific surface wind and SST anomalies.

The sudden establishment of the Philippine Sea anticyclone and the concurrent enhancement of the cooling east of the anticyclone suggest that the development of air-sea coupling and the associated wind and SST anomalies can take place within a month. This is likely triggered by atmospheric processes, such as an intrusion of an excessively strong cold surge from mid-latitudes. The previous winter monsoon experiments have shown the effectiveness of the cold airmass transformation over warm ocean surfaces through sensible heat exchange (Johnson and Zimmermann 1986). The ocean may lose a considerable amount of heat due to enhanced outgoing buoyancy fluxes and enhanced entrainment in the ocean mixed layer. Both the significant drop in SST and excitation of the atmospheric Rossby waves can occur in a couple of weeks. This may explain the rapidness of the concurrent enhancement of the cooling and the surface anticyclone in the WNP.

b. Seasonal dependence of the WNP wind anomalies and ENSO turnabouts

The positive feedback between the atmospheric Rossby wave and ocean mixed layer thermodynamics occurs only when mean northeasterly trades prevail in the western North Pacific. This favorable mean state happens only from late fall through the next spring. Thus, the atmosphere-ocean thermodynamic interaction, which generates and maintains the western North Pacific wind anomalies, depends critically on the presence of the boreal cold season (from October to May) mean surface winds.

We have speculated that the rapid establishment of the anticyclone and associated enhancement of western Pacific cooling is likely triggered by strong cold surges over the

Philippine Sea and followed by an effective interaction between the surface anticyclone and the local cooling through wind-evaporation-SST feedback. The normal intrusion of cold surges occurs over the South China Sea (Chang and Lau 1982). An intrusion of cold surges into the Philippine Sea and western North Pacific requires an abnormal eastward shift of the westerly jet. The strong central Pacific warming generally plays such a role. The central Pacific warming enhances the subtropical anticyclone and induces an eastward shift and intensification of the Aleutian Low and associated westerly jet—the Pacific-North American (PNA) teleconnection (Wallace and Gutzler 1981). Associated with the eastward shift of the Aleutian Low, the pressure rises east of Japan (Wang et al. 1999b). This anomalous large scale circulation favors intrusion of cold surges into the Philippine Sea. Thus, the central Pacific warming sets up an environment which is conducive to the effective air-sea interaction in the WNP. The latter leads to the rapid development of the western Pacific cooling and the Philippine Sea anticyclone. Note, however, that the occurrence of the PNA pattern is associated with forced Rossby wave trains (Hoskins and Karoly 1981) and the baroclinic instability of the midlatitude westerlies (Simmons et al. 1983), both of which depend on the boreal winter mean circulation. Therefore, the tropical-extratropical interaction that is needed for the rapid establishment of the WNP wind and SST anomalies can occur only in boreal winter.

In summary, both the atmosphere-ocean interaction and the tropical-extratropical interaction, which are critical to the rapid development and maintenance of the WNP wind and SST anomalies, depend on the boreal winter mean circulation. Therefore, the WNP wind anomalies associated with ENSO have strong seasonality. Prominent anticyclonic (cyclonic) anomalies associated with the ENSO warming (cooling) develop preferably in late fall. As a result, the turnabouts from warming to cooling or vice versa would tend to take place in late

boreal fall to early winter and the reversed trends continue throughout the following spring. This provides a plausible explanation for the phase-lock of ENSO turnabouts to the annual cycles.

4. Impacts of the western Pacific wind anomalies on ENSO turnabouts

The observational evidence presented in section 2 suggests that the WNP variability may have a significant impact on ENSO turnabouts. In this section, we use a coupled ocean-atmosphere model to examine the impacts of the western Pacific wind anomalies on ENSO turnabouts.

The intermediate coupled model of Zebiak and Cane (1987) (hereafter the CZ model) is a useful tool for understanding the basic dynamics of ENSO. In the CZ model, the mean states of the atmosphere and ocean are specified, which have fundamental controls on the model ENSO behavior. For given model parameters and specified basic states described in Zebiak and Cane (1987), the model exhibits an irregular oscillation with a period about of 48 months. The warm peak tends to occur around November, while the cold peaks occur most frequently from July to September. The former agrees with, but the latter is at odds with the observations. Explanation of the mechanisms of the phase lock in the CZ model is beyond the scope of the present study.

Our interest is to identify roles of the seasonally-dependent WNP wind anomalies in ENSO turnabouts using a credible coupled model. To achieve our goal, we need to modify the CZ model. The modification is necessary, because the atmospheric component of the CZ model is not able to reproduce observed wind anomalies in the western Pacific (Fig. 10a). Figure 10a shows the model wind anomalies associated with the principal eigenvector calculated using the singular value decomposition (SVD) method (Bretherton et al. 1992) applied to SST and wind

anomalies obtained from an output of a 200-year integration of the CZ model. Figure 10a shows that in the CZ model the wind anomalies to the west of the dateline are negligibly small. In addition, wind anomalies in the western Pacific do not have appreciable seasonal variations (Fig. 11a). These deficiencies result from the incomplete physics of the CZ atmospheric model.

In order to realistically represent western Pacific wind anomalies in the atmospheric model, we used an empirical atmospheric model that is derived using the SVD method applied to FSU observed wind stress anomalies (Goldenberg and O'Brien 1981) and NCEP (Kalnay et al. 1996) SST anomalies. The anomalous wind response to particular SST anomalies varies with the seasonal mean states. To capture this seasonal dependence, the SVD modes are computed using SST and wind anomaly data that are stratified by calendar month. Thus, the derived SVD modes have significant seasonal variations. To illustrate the seasonally-dependent part of the wind anomalies, we decompose the first leading SVD modes into an annual mean (Fig. 10b) and an annual cycle component (Fig. 11b). The annual mean component represents a mean atmospheric response to the tropical Pacific SST anomalies averaged over all seasons. It is quite similar to the spatial pattern observed during the composite mature phase of the El Niño events (Rasmusson and Carpenter 1982). The wind anomalies in the empirical model display a maximum westerly in the central Pacific along with pronounced equatorward convergent winds in the South Pacific Convergence Zone. Compared with the CZ atmospheric model, there is a systematic westward shift of phase in both the SST and wind anomalies in the empirical model.

In the empirical atmospheric model, the wind anomalies exhibit significant seasonality that can be seen from the annual cycle component of the leading SVD modes (Fig. 11b). Prominent annual variations in the wind anomalies are found in the WNP. A seasonal reversal of the surface wind stress is evident, indicating that the empirical model reflects well the boreal

winter anticyclonic (cyclonic) wind anomalies in the WNP during an El Niño (La Niña). In response to the mature phase of ENSO warming which usually occurs in boreal winter, the WNP wind anomalies display an anticyclonic vorticity from December to May. The annual modulation of wind anomalies in the eastern Pacific Inter-tropical Convergence Zone can also be seen in Fig. 11b. The prominent interannual oscillation in the empirical atmosphere model allows for an investigation of the impacts of the western Pacific wind anomalies on ENSO.

To test the sensitivity of the ENSO cycle to the seasonal variation of the western Pacific wind anomalies, we use a modified CZ model. Here, the empirical atmosphere is formulated using the first two SVD modes that account for about 85% of the total covariance between SST and winds. The coupling parameters used for the modified couple model are the same as in the CZ model. Similar to the CZ model, both the atmospheric and oceanic mean states are specified in the modified CZ model. Figure 12 shows a time series of the NINO3 SST anomalies obtained from a control experiment using the modified CZ model. The period of interannual oscillation is about 37 months, which is shorter than in the original CZ model (48 months) for the same set of model parameters. The shortened oscillation period is consistent with the delayed oscillator theory, because the westward wind shift of the maximum equatorial westerly anomalies reduces the time for the off-equatorial Rossby waves to affect the thermocline in the equatorial eastern Pacific.

In order to identify the impacts on ENSO cycles of the seasonality in the wind response, we compare the results derived from experiments in which the seasonally-independent wind anomalies (the annual mean SVD modes, τ_A) and the seasonally-dependent wind anomalies (the annually varying SVD modes, τ_s) are used. In particular, to isolate the effect of the wind anomalies in the western Pacific and in the eastern Pacific respectively, we designed two

additional versions of the empirical atmospheric model. In the active western Pacific run,

$$\tau_w = w\tau_s + (1-w)\tau_A, \tag{4.1}$$

while in the active eastern Pacific run,

$$\tau_E = (1-w)\tau_s + w\tau_A, \tag{4.2}$$

where the weighting function is defined as

$$w(x) = \begin{cases} 1, & x < 180^\circ E; \\ (200 - x)/20, & 180^\circ E < x < 200^\circ E; \\ 0, & x > 200^\circ E. \end{cases}$$

Here x is the longitude (for convenience, the longitude east of the dateline is converted to an eastern longitude, i.e., 200°E=160°W). In the active western Pacific run, τ_W, we retain only the seasonality of the wind anomaly in the western Pacific. On the other hand, in the active eastern Pacific wind model, τ_E, we retain only the seasonal variations of the eastern Pacific wind anomalies. Similarly, to identify the role of the ocean basic state, we compare the results derived using the annual mean and annual cycle of the ocean basic state. An array of numerical experiments with different combinations of the basic states was designed. Table 1 summarizes the main features of these experiments. In each numerical experiment the coupled model was integrated with the same initial condition and the same model parameters for a period of 100 years. The calendar months associated with the peaks of both El Niño and La Niña are counted and the dominant period is determined, both using NINO3 SST anomalies. The results are shown in Fig. 13 and summarized in Table 1.

When the ocean basic state is fixed at the annual mean state and the seasonally-independent atmospheric model is used, the coupled model exhibits a regular oscillation with a period of about 37 months. This represents the intrinsic interannual oscillation of the coupled

system in the absence of the influences from the annual cycle basic state. As expected, in this case the phase of the model ENSO cycle is randomly distributed throughout the year (Fig. 13a and Table 1).

When the empirical atmospheric model, which contains the annual variation of the wind anomalies in the *western* Pacific (active western Pacific run), is used while the ocean basic state remains the annual mean, the coupled model exhibits a 3-year oscillation. The warm and cold peaks are precisely phase-locked to the annual cycle with warm peaks occurring in November and January and cold peaks in November (Fig. 13b). This phase-lock agrees with observations. In contrast, when the empirical atmospheric model, which contains the annual variation of the wind anomalies in the *eastern* Pacific only (active eastern Pacific run), along with the annual mean ocean basic state is used, the coupled model shows an irregular oscillation with a period of about 37 months. Most warm and cold peaks in this experiment occur in May-July and in March-May (Fig. 13c), respectively. The phase-locking in this experiment is totally at odds with observations. Since these two experiments exclude the annual cycle in the ocean basic state, they isolate the impacts of the annual variations of the wind anomalies in the western Pacific and eastern Pacific, respectively. Obviously, the annual variation in the western Pacific yields realistic ENSO phase-locking behavior, whereas the annual variations in the eastern Pacific wind anomalies alone do not. When the seasonally-dependent empirical atmospheric model along with the annual mean ocean basic state were used, the coupled model exhibits a 37-month oscillation with the warm peaks in November and May and the cold peaks in May-July (Fig. 13d), respectively. This phase behavior results from a mixed effect of the seasonally-dependent wind responses in both the western and the eastern Pacific.

The results in the above three experiments indicate that the seasonal dependence of the

western Pacific wind anomalies (mainly in the WNP) has a positive contribution to the phase-locking behavior of the model ENSO. This suggests that the seasonallly-dependent response of the western Pacific wind anomalies, which is originated in association with boreal winter mean trade winds, may be a contributor to locking ENSO turnabouts to boreal winter.

The role of the annual cycle of the ocean basic state cannot be ruled out. When the model ocean mean state includes an annual cycle (while the empirical atmosphere excludes seasonal variation), the oscillation is irregular with a period of 37 months. The model ENSO warm peaks occur in November to January, while the cold peaks scatter in the later part of the year from July to December (Fig. 13e). This indicates that the ocean annual cycle not only creates low-order chaos but also favors a phase-lock of the warm peaks to the boreal winter. However, the phases of cold peaks are not well locked to the annual cycle.

In the active western Pacific run with the annual cycle of the ocean basic state, the resultant oscillation period is again exactly 3 years. Both the warm and cold peaks are precisely phase-locked to the annual cycle with warm peaks occurring in December and cold peaks in November (Fig. 13f). Therefore, the seasonally dependent wind anomalies in the western Pacific not only reinforce the phase-lock of the warm peak to boreal winter, but also correct the timing of cold peak occurrence. On the other hand, the seasonal variation of the eastern Pacific wind anomalies does not improve the timing of the cold phase: the cold peaks occur in June, August, and January (Fig. 13g). When both the ocean annual cycle and the seasonal variations of the wind anomalies are included (in the control experiment), the coupled system displays a stronger phase-lock (Fig. 13h); both the warm and cold peaks occur in boreal winter (November and December).

The results obtained from the above sensitivity tests show that both the annual variations

in the atmospheric winds and the annual cycle in oceanic mean states contribute to the phase-lock of ENSO extrema to the annual cycle. Their combined effect yields a strong tendency for the warm or cold peaks to occur toward the end of the calendar year. In the presence of the ocean annual cycle but without the seasonality in the wind anomalies, the phases of the cold peaks are not well locked to the annual cycle. On the other hand, in the presence of the seasonal variations of the anomalous winds in the western Pacific, both the warm and cold peaks are tightly locked to the boreal winter regardless of the presence of the annual cycle of the ocean basic state. In this coupled model, the western Pacific wind variations appear to be more important than the annual cycle of the ocean mean state in producing the phase-locking behavior of ENSO.

5. Conclusion and discussion

We have shown that the turnabouts from basin-wide warming to cooling or vice versa during strong El Niño (La Niña) events are preceded by a rapid establishment of an *anomalous anticyclone (cyclone)* over the Philippine Sea. The associated zonal wind anomalies extend to the equatorial western Pacific, which directly forces upwelling (downwelling) equatorial Kelvin waves, providing a negative feedback to the coupled system. Furthermore, the coherent variations in the wind and SST in the WNP indicate a local positive feedback arising from *in situ* air-sea interaction through thermodynamical coupling. The development and maintenance of the Philippine Sea wind anomalies are attributed to this positive feedback. The critical processes for the rapid development and maintenance of the WNP wind anomalies during the extreme phases of ENSO cycles, i.e., the ocean-atmosphere interaction and tropical-extratropical interaction, rely on the boreal winter background states. Thus, this negative feedback mechanism favors an

occurrence of the ENSO turnabouts toward the end of the calendar year.

The numerical experiments with a modified Zebiak and Cane (1987) model demonstrate that the seasonal dependence of the western Pacific wind anomalies plays an important role in reversing the warming and cooling trends in boreal winter. Without this seasonality the coupled model could not reproduce the observed preferred occurrence of the cold peaks in boreal winter.

The positive feedback between the Philippine Sea anticyclone and SST depends not only on the seasonal cycle but also on the Central Pacific SST anomalies. As we pointed out previously, there is one strong warm event (1986-87) which failed to reverse the warming trend by the end of the ENSO developing year (the boreal winter of 1986-87). Inspection of the western Pacific wind anomalies indicates that the easterly anomalies in the equatorial western Pacific were not well established and did not persist in the boreal winter of 1986-87 (Fig. 14). There is a notable difference between the 1986-87 event and the other six strong events shown in Fig. 2. The 1986-87 warming started in the fall of 1986. Toward the end of 1986, the monthly mean NINO 3.4 SST anomalies were well below 1.5 standard deviations, whereas during the other six strong events, the NINO 3.4 SST anomalies were above 1.5 standard deviations by the end of the ENSO development year. Scenarios similar to the 1986-87 event are found during two other moderate prolonged warm events of 1968-69 and 1976-77. An important feature common to all three prolonged events is the insufficient strength of the central Pacific warming (NINO 3.4 SST anomalies less than 1.5 standard deviation) toward the end of the ENSO development year. This suggests that the strong warming in the equatorial central Pacific is necessary for the rapid establishment of the western Pacific wind anomalies.

The proposed mechanism is derived from an analysis of *major* warm (cold) events during which the central Pacific warming reaches certain strength. Compared to strong ENSO events,

the moderate and weak events tend to have a looser phase-locking tendency. The numerical experiments suggest that the proposed mechanism is not the only one responsible for the ENSO turnabout, but may significantly contribute to the boreal winter reversal of the warming or cooling trends. The annual variation in the ocean mean states can also have an important bearing on the ENSO phase-lock to the annual cycle.

Note that the enhancement of the equatorial westerlies is not always concurrent with the decrease of the Philippine Sea cyclone (Fig. 2b), suggesting that some of the events of enhanced westerlies may be affected by the equatorial eastward propagation of the zonal wind anomalies associated with the Madden-Julian Oscillation. This deserves further study in the future.

The processes important for the air-sea interaction and tropical-extratropical interaction in the off-equatorial western Pacific have not been systematically monitored. It is unknown how well the coupled ocean-atmospheric general circulation models simulate these processes during ENSO turnabouts. Some of the forecast models which were successful in prediction of the development of 1997-98 ENSO failed to predict the sharp reversal of the trend in early 1998 (NOAA/NCEP Climate Diagnostic Bulletin). The proposed mechanism calls for further in-depth studies of ENSO dynamics using observations with higher temporal resolution and larger spatial extent and using more reliable coupled intermediate and general circulation models.

Acknowledgements:

This research has been supported by grants to the University of Hawaii by NOAA OGP and by the NSF grant ATM96-13776. R. Lukas was supported by NSF grant OCE95-25986. The International Pacific Research Center is sponsored in part by the Frontier Research System for Global Change. This is SOEST publication No XXXX and IPRC publication No XXXX.

REFERENCES

Battisti, D. S., and A. C. Hirst, 1989: Interannual variability in the tropical atmosphere-ocean system: Influence of the basic state and ocean geometry. *J. Atmos. Sci*., **46**, 1687-1712.

Bretherton, C. S., S. Smith, and J. M. Wallace, 1992: An intercomparison of methods for finding coupled patterns in climate data. *J. Climate*, **5**, 541-560.

Cane, M. A., M. Münnich, and S. E. Zebiak, 1990: A study of self-excited oscillations in a tropical ocean-atmosphere system. Part I: Linear analysis. *J. Atmos. Sci*., **47**, 1562-1577.

Chang, C.-P., and K.-M. Lau, 1982: Short-term planetary scale interactions over the tropics and midlatitudes during northern winter. Part I: Contrasts between active and inactive periods. *Mon. Wea. Rev*., **110**, 933-946.

Chao, Y., and S. G. H. Philander, 1993: On the structure of the Southern Oscillation. *J. Climate*, **6**, 450-469.

Deser, C., and J. M. Wallace, 1990: Large-scale atmospheric circulation features of warm and cold episodes in the tropical Pacific. *J. Climate*, **3**, 1254-1280.

Eriksen, C. C., M. B. Blumenthal, S. P. Hayes, and P. Ripa, 1983: Wind generated equatorial Kelvin waves observed across the Pacific Ocean. *J. Phys. Oceanogr*., **13**, 1622-1640.

Fu, X., and B. Wang, 1999: On the role of longwave radiation and boundary layer thermodynamics in forcing tropical surface winds. *J. Climate*, **12**, 1049-1069.

Goldenberg, S. B., and J. J. O'Brien, 1981: Time and space variability of tropical Pacific wind stress. *Mon. Wea. Rev.*, **109**, 1190-1207.

Harrison, D. E., and N. K. Larkin, 1996: The COADS sea level pressure signals: A near-global El Niño composite and time series view, 1946-1993. *J. Climate*, **9**, 3025-3055.

Hirst, A. C., 1986: Unstable and damped equatorial modes in simple coupled ocean-atmosphere models. *J. Atmos. Sci*., **43**, 606-630.

Hoskins, B. J., and D. J. Karoly, 1981: Planetary-scale atmospheric phenomena associated with the Southern Oscillation. *Mon. Wea. Rev*., **109**, 813-829.

Ji, M., A. Leetmaa, and J. Derber, 1995: An ocean analysis system for seasonal to interannual climate studies. *Mon. Wea. Rev.*, **123**, 460-481.

Johnson, R. H., and J. R. Zimmermann, 1986: Modification of the boundary layer over the South China Sea during a winter MONEX cold surge event. *Mon. Wea. Rev*., **114**, 2004-2015.

Kalney, E., and Coauthors, 1996: The NCEP/NCAR 40-year reanalysis project. *Bull. Amer. Meteor. Soc.,* **77**, 437-471.

Kessler, W. S., and M. J. McPhaden, 1995: Oceanic equatorial waves and the 1991-1993 El Niño. *J. Climate*, **8**, 1757-1774.

Kirtmann, B. P., and D. G. DeWitt, 1997: Comparison of atmospheric model wind stress with three different convective parameterizations: Sensitivity of tropical Pacific Ocean simulations. *Mon. Wea. Rev*., **125**, 1231-1250.

Knox, R. A., and D. Halpern, 1982: Long range Kelvin wave propagation of transport variations in Pacific Ocean equatorial currents. *J. Mar. Res*., **40** (suppl.), 329-339.

Li, B., and A. J. Clarke, 1994: An examination of some ENSO mechanisms using interannual sea level at the eastern and western equatorial boundaries and the zonally averaged equatorial wind. *J. Phys. Oceanogr.*, **24**, 681-690.

Lukas, R., S. P. Hayes, and K. Wyrtki, 1984: Equatorial sea level response during the 1981-1983 El Niño. *J. Geophys. Res*., **89**, 10425-10430.

Mayor, D. A., and R. H. Weisberg, 1998: El Niño-Southern Oscillation-related ocean-

atmosphere coupling in the western equatorial Pacific. *J. Geophys. Res.*, **103**, 18635-18648.

McPhaden, M. J., and X. Yu, 1999: Genesis and evolution of the 1997-98 El Niño. *Science*, **283**, 950-954.

Philander, S. G. H., and E. M. Rasmusson, 1985: The Southern Oscillation and El Nino. *Adv. Geophys*., **28A**, 197-215.

Philander, S. G. H., T. Yamagata, and R. C. Pacanowski, 1984: Unstable air-sea interactions in the tropics. *J. Atmos. Sci.*, **41**, 604-613.

Picaut, J., M. Loualalen, C. Menkes, T. Delcroix, and M. J. McPhaden, 1996: Mechanism of the zonal displacements of the Pacific warm pool: Implications for ENSO. *Science,* **274**, 1486-1489.

Rasmusson, E. M., and T. H. Carpenter, 1982: Variations in tropical sea surface temperature and surface wind fields associated with the Southern Oscillation/ El Niño. *Mon. Wea. Rev*., **110**, 354-384.

Schopf, P. S., and M. J. Suarez, 1988: Vacillations in a coupled ocean-atmosphere model. *J. Atmos. Sci.*, **45**, 549-566.

Simmons, A., J. M. Wallace, and G. W. Branstator, 1983: Barotropic wave propagation and instability, and atmospheric teleconnection patterns. *J. Atmos. Sci.*, **40**, 1363-1392.

Suarez, M. J., and P. S. Schopf, 1988: A delayed action oscillator for ENSO. *J. Atmos. Sci*., **45**, 3283-3287.

Tziperman, E., M. A. Cane, S. E. Zebiak, Y. Xue, and B. Blumenthal, 1998: Locking of El Niño's peak time to the end of calender year in the delayed oscillator picture of ENSO. *J. Climate*, **11**, 2191-2199.

Wallace, J. M., and D. S. Gutzler, 1981: Teleconnections in the geopotential field during the Northern Hemisphere winter. *Mon. Wea. Rev.*, **109**, 784-812.

Wang, B., 1995a: Interdecadal changes in El Nino onset in the last four decades. *J. Climate*, **8,** 267-285.

Wang, B., 1995b: Transition from a cold to a warm state of the El Niño-Southern Oscillation cycle. *Meteor. Atmos. Phys.*, **56**, 17-32.

Wang, B., and Z. Fang, 1996: Chaotic oscillations of tropical climate: A dynamic system theory for ENSO. *J. Atmos. Sci.*, **53**, 2786-2802.

Wang, B., and T. Li, 1993: A simple tropical atmosphere model of relevance to short-term climate variations. *J. Atmos. Sci*., **50**, 260-284.

Wang, B., R. Wu, and X. Fu, 1999a: Pacific-East Asian Teleconnection: How does ENSO affect East Asian climate? *J. Climate*, In press.

Wang, B., R. Wu, and R. Lukas, 1999b: Roles of the western North Pacific wind variation in thermocline adjustment and ENSO phase transition. *J. Meteor. Soc. Japan*, **77**, 1-16.

Weisberg, R. H., and C. Wang, 1997: Slow variability in the equatorial west-central Pacific in relation to ENSO. *J. Climate*, **10**, 1998-2017.

Woodruff, S. D., R. J. Sultz, R. L. Jenne, and P. M. Steurer, 1987: A comprehensive ocean-atmosphere data set. *Bull. Amer. Meteor. Soc.*, **68**, 1239-1250.

Zebiak, S. E., and M. A. Cane, 1987: A model El Niño-Southern Oscillation. *Mon. Wea. Rev*., **115**, 2262-2278.

Table 1 Description of main features and the results in the sensitivity experiments. The symbols W and C refer to the warm and cold peaks, respectively.

	Ocean basic state	
	Annual mean	Annual cycle
Seasonally-independent atmospheric model	-37 months -No phase-locking	-37 months -W(Dec), C(Jul-Dec)
Active Western Pacific run	-3 years -W(Jan, Nov), C(Nov)	-3 years -W(Dec), C(Nov)
Active Eastern Pacific run	-37 months -W(May-Jul), C(Apr-May)	-40 months -W(Nov), C(Jun, Aug, Jan)
Seasonally-dependent atmospheric model	-37 months -W(Nov), C(Jun)	-37 months -W(Nov), C(Dec)

Figure Captions

Fig. 1 Monthly mean SST anomalies averaged in the NINO 3.4 region (5°S-5°N, 170-120°W). The SST data are derived from the National Center for Environmental Prediction (NCEP) reanalysis (Kalnay et al. 1996) except for 1957 which is derived from Comprehensive Ocean-Atmosphere Data Set (COADS) (Woodruff et al. 1987). The dashed horizontal lines indicate 1.5 times standard deviation of the SST anomalies.

Fig. 2 Time series of selected ENSO anomalies around the mature phases of the six strongest warm (a) and the five strongest cold (b) episodes during the period of 1957-1998. The abscissa denotes a time window spanning 18 months centered around November of the years during which warm (cold) events reach a mature phase. The solid curves show NINO3.4 (5°S-5°N, 120-170°W) SST anomalies (°C). The dashed and dotted curves show, respectively, sea level pressure anomalies (hPa) over the Philippine Sea (10-20°N, 120-150°E) and surface zonal wind anomalies (m/s) north of New Guinea (4°S-4°N, 120-150°E). The surface wind data are derived from COADS (Woodruff et al. 1987). The black dots denote the times of peak warm (cold) SST anomalies.

Fig. 3 Composite SST anomalies (°C) in NINO3.4 region (solid curves), sea level pressure anomalies (hPa) over the Philippine Sea (dashed curves), and surface zonal wind anomalies (m/s) north of New Guinea (dotted curves) for the six major warm (a) and the five major cold (b) events on Fig. 2. The composite is made according to the peak warm (cold) months with the abscissa denoting the lag time (month) with respect to the time of peak warm (cold).

Fig. 4 Monthly tendency of 1000 hPa winds at one month prior to the peaks of the six major warm episodes. The wind scale is indicated on the upper right corner of the panels. The data are

from NCEP reanalysis except for 1957 which is from COADS.

Fig. 5 Composite sea level pressure and 1000 hPa monthly mean wind tendencies at one month prior to the peak warm for the five major warm events (excluding 1957/58) (a) and at two month prior to the peak cold for the five major cold events (b) on Fig. 2. The contour interval is 1 hPa. The wind scale is indicated between the two panels. Shading indicates regions where the wind tendency differences between (a) and (b) are significant at a 95% confidence level according to the Student t-test.

Fig. 6 Monthly mean local rates of change (°C/month) of subsurface ocean temperature in a vertical section along the equator during the turnabouts of (a) the 1982/83 warm event (December 1982-May 1983) and (b) the 1991/92 warm event (December 1991-May 1992). The ordinate denotes the depth (m) below the surface. The thick dashed lines are the 20°C isotherm, showing the mean position of the thermocline during that month. The contour interval is 1 °C/month.

Fig. 7 Similar to Fig. 6 except for (a) the 1984/85 cold event (October 1984-March 1985) and (b) the 1988/89 cold event (October 1988-March 1989) with the contour interval of 0.5 °C/month.

Fig. 8 Composite SST and 1000 hPa wind anomalies during the reversal of the warming trend from 3 months before (lag=-3) to 4 months after (lag=+4) the warm peak. The contour interval is 0.2°C. Shading denotes SST anomalies less than -0.4°C. The wind scale is given at the upper-right corner of the panels.

Fig. 9 Hovemöller diagrams of composite SST (°C) and 1000 hPa wind anomalies (m/s) along 5-15°N (a) and sea level pressure anomalies (hPa) along 10-20°N (b) for the six major warm events. The composite is centered on the peak warm months. The ordinate is the lag time (month) with respect to the warm peak.

Fig. 10 Annual mean component of the first SVD vectors of surface wind stress and SST anomalies derived from the results of the CZ model control run (a) and the observed data (b). . The SVD analyses are performed for each calendar month. Unit of SST anomaly is ºC. The vector scale is displayed at the top right corner.

Fig. 11 Similar to Fig. 10 except for the annual cycle component. The calendar month is indicated at the top left corner of each panel.

Fig. 12 Time series of NINO3 SST anomaly calculated in a control experiment using the hybrid (empirical atmosphere and Cane-Zebiak ocean) coupled model.

Fig. 13 Histograms of the percentage of warm (filled bar) and cold (blank bar) peaks for eight experiments described in Table 1. The percentage is calculated by the ratio of warm (cold) peaks in each month divided by the total warm (cold) peaks in the entire calendar year.

Fig. 14 Monthly mean SST anomalies (°C) in the NINO 3.4 region (solid curve) and surface zonal wind anomalies (m/s) north of New Guinea (4°S-4°N, 120-150°E) during 1986-1988.

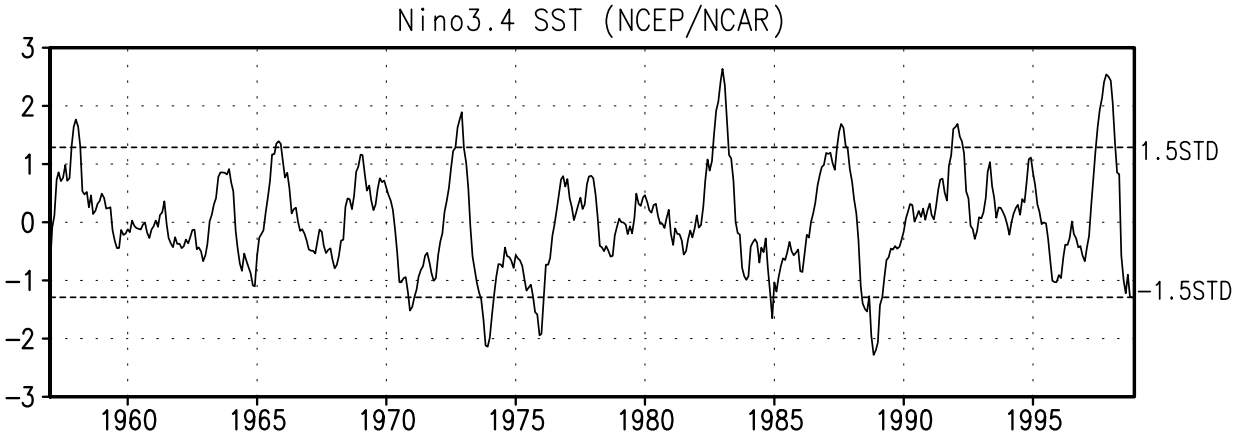
Nino3.4 SST (NCEP/NCAR)
3
2
1
0
−1
−2
−3
1.5STD
−1.5STD
1960
1965
1970
1975
1980
1985
1990
1995

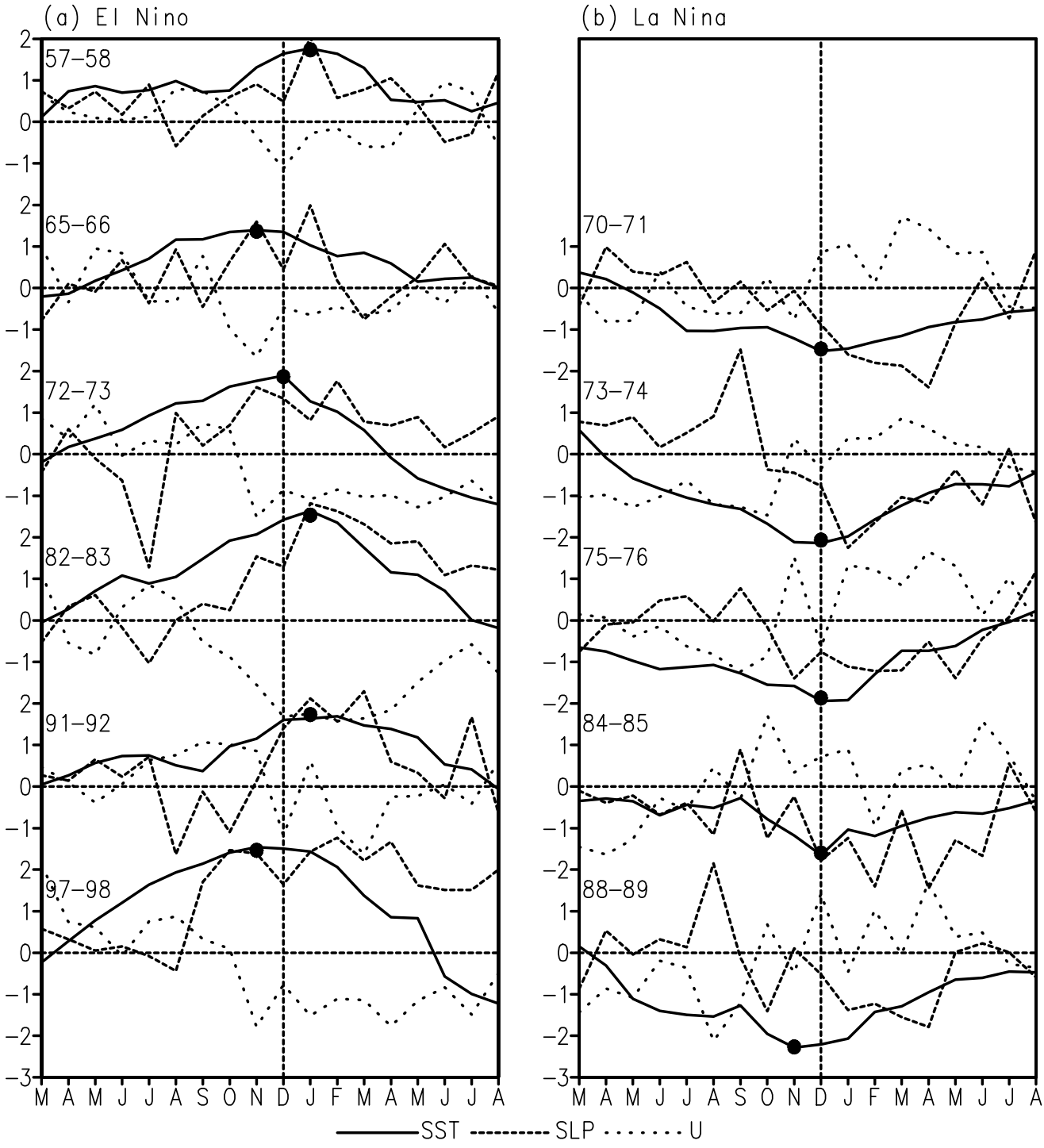
(a) El Nino
(b) La Nina
57–58
65–66
72–73
82–83
91–92
97–98
70–71
73–74
75–76
84–85
88–89
M A M J J A S O N D J F M A M J J A
SST
SLP
U

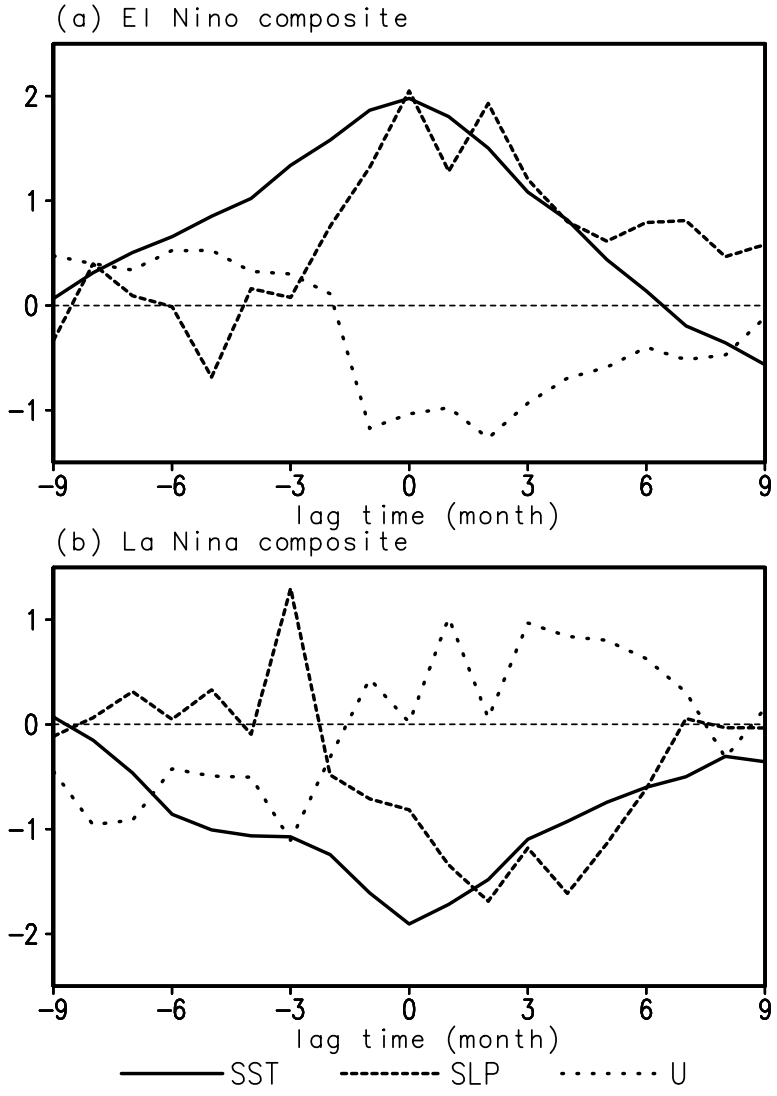
(a) El Nino composite
2
1
0
−1
−9
−6
−3
0
3
6
9
lag time (month)
(b) La Nina composite
1
0
−1
−2
−9
−6
−3
0
3
6
9
lag time (month)
SST
SLP
U

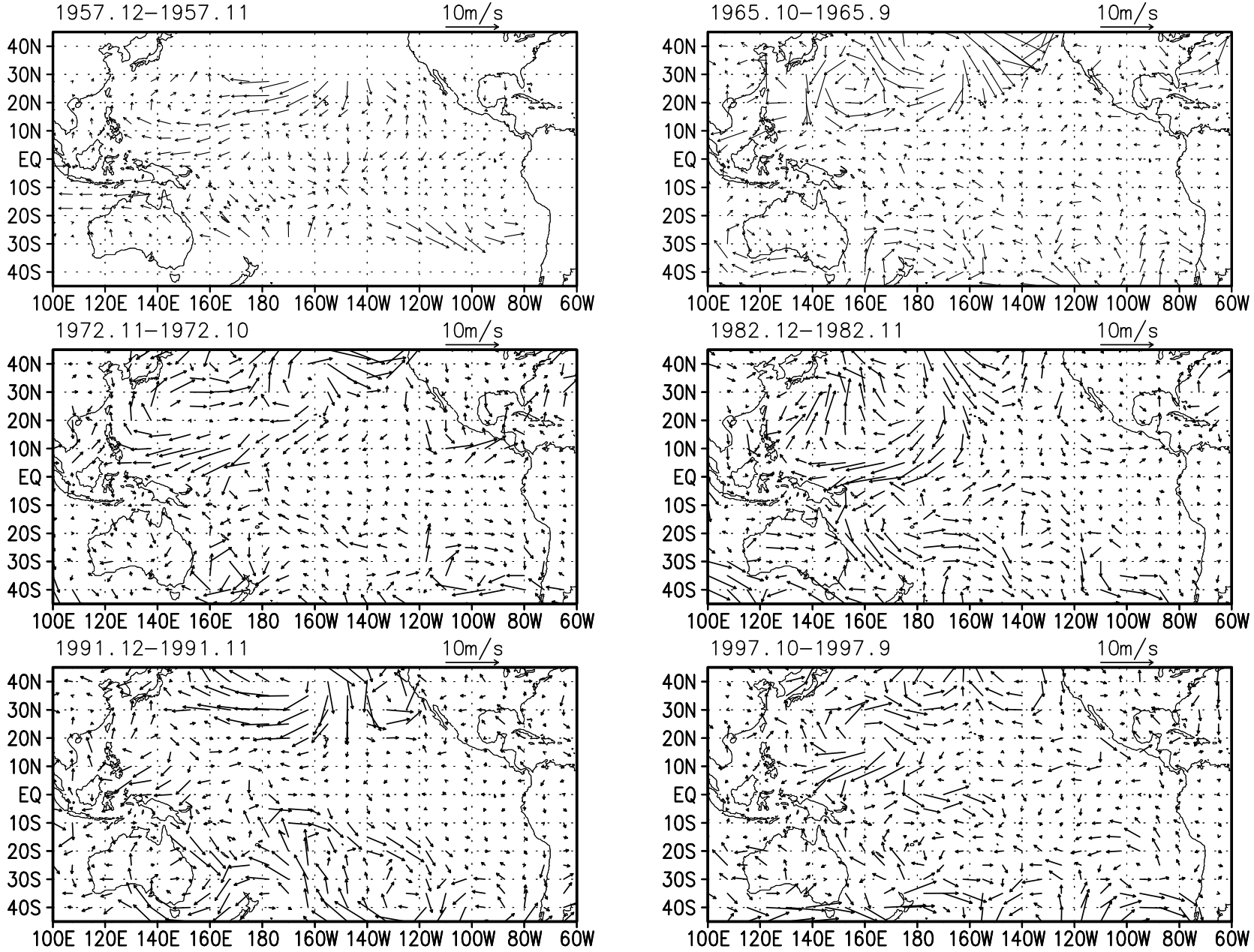
1957.12–1957.11
10m/s
1965.10–1965.9
10m/s
1972.11–1972.10
10m/s
1982.12–1982.11
10m/s
1991.12–1991.11
10m/s
1997.10–1997.9
10m/s
40N
30N
20N
10N
EQ
10S
20S
30S
40S
100E 120E 140E 160E 180 160W 140W 120W 100W 80W 60W

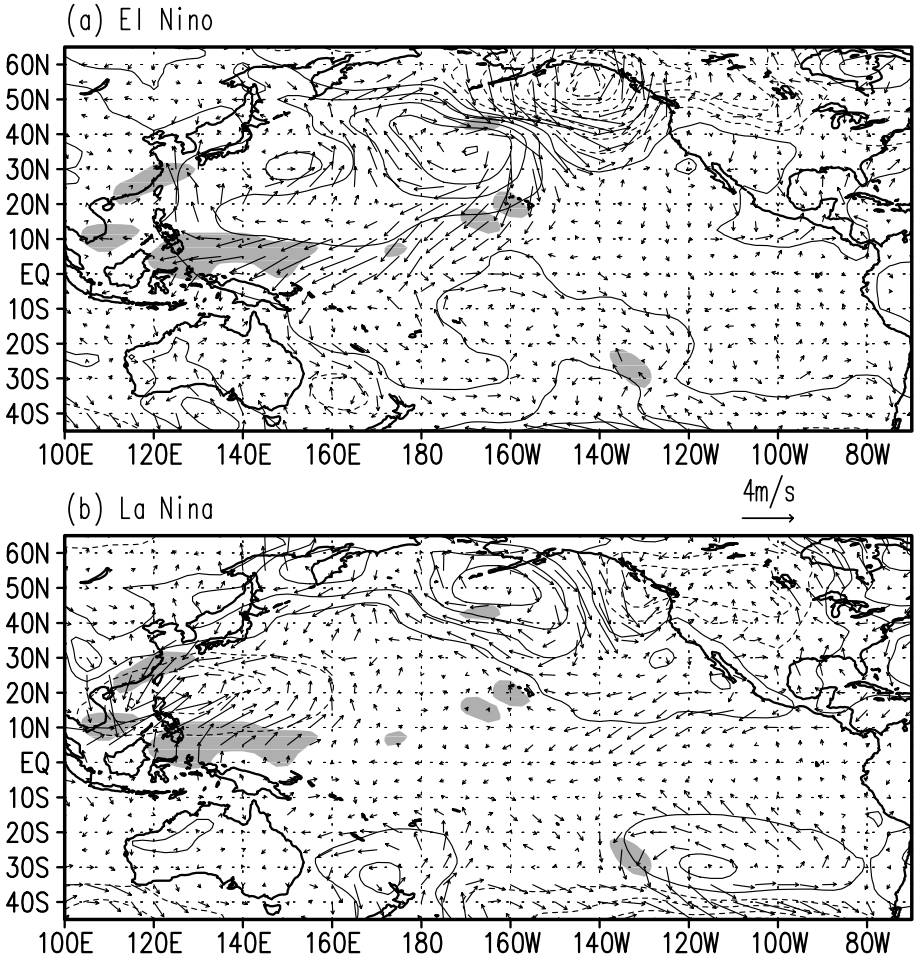
(a) El Nino
60N
50N
40N
30N
20N
10N
EQ
10S
20S
30S
40S
100E
120E
140E
160E
180
160W
140W
120W
100W
80W
4m/s
(b) La Nina
60N
50N
40N
30N
20N
10N
EQ
10S
20S
30S
40S
100E
120E
140E
160E
180
160W
140W
120W
100W
80W

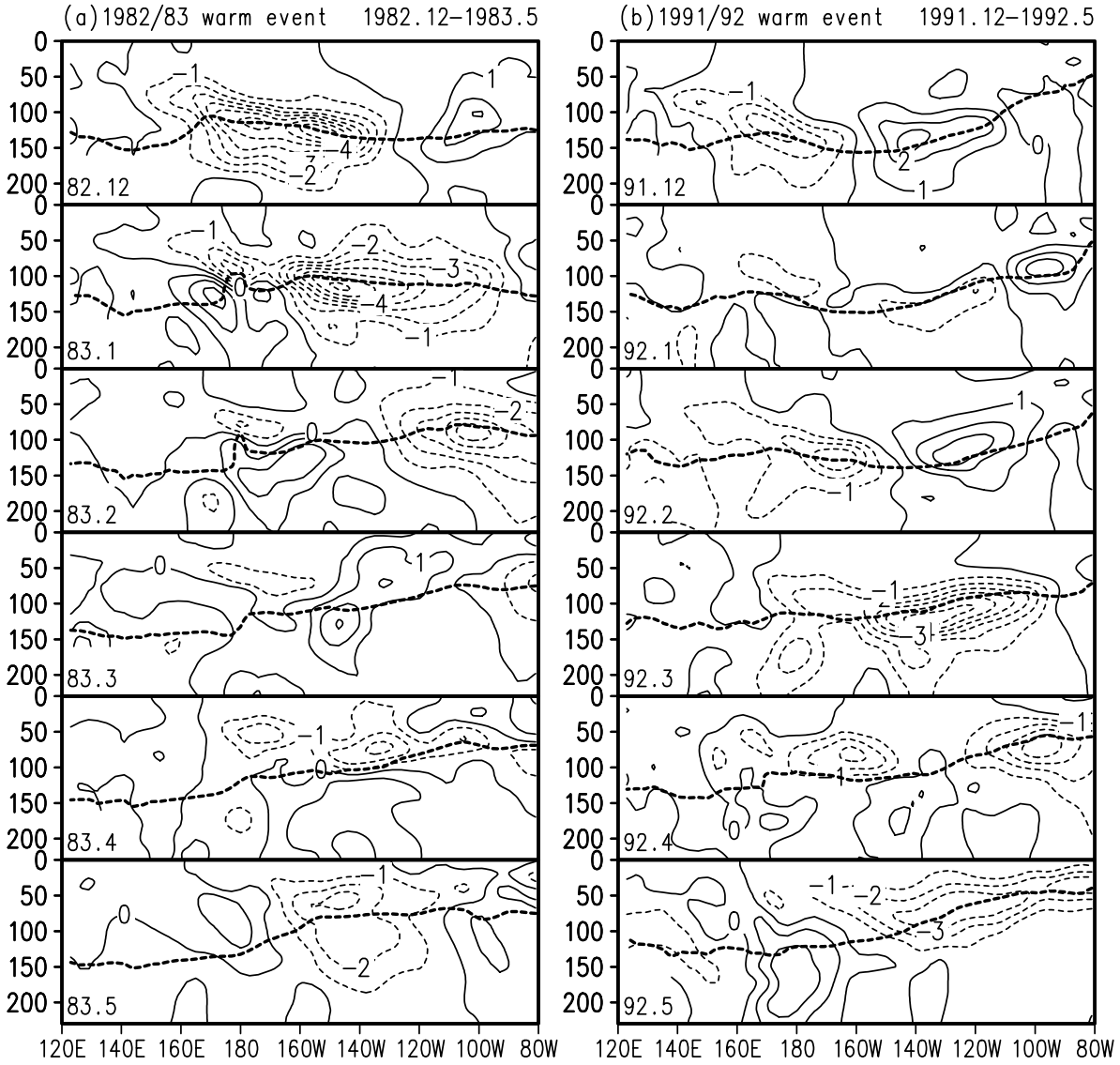
(a)1982/83 warm event 1982.12–1983.5
(b)1991/92 warm event 1991.12–1992.5
82.12
83.1
83.2
83.3
83.4
83.5
91.12
92.1
92.2
92.3
92.4
92.5
0
50
100
150
200
120E 140E 160E 180 160W 140W 120W 100W 80W

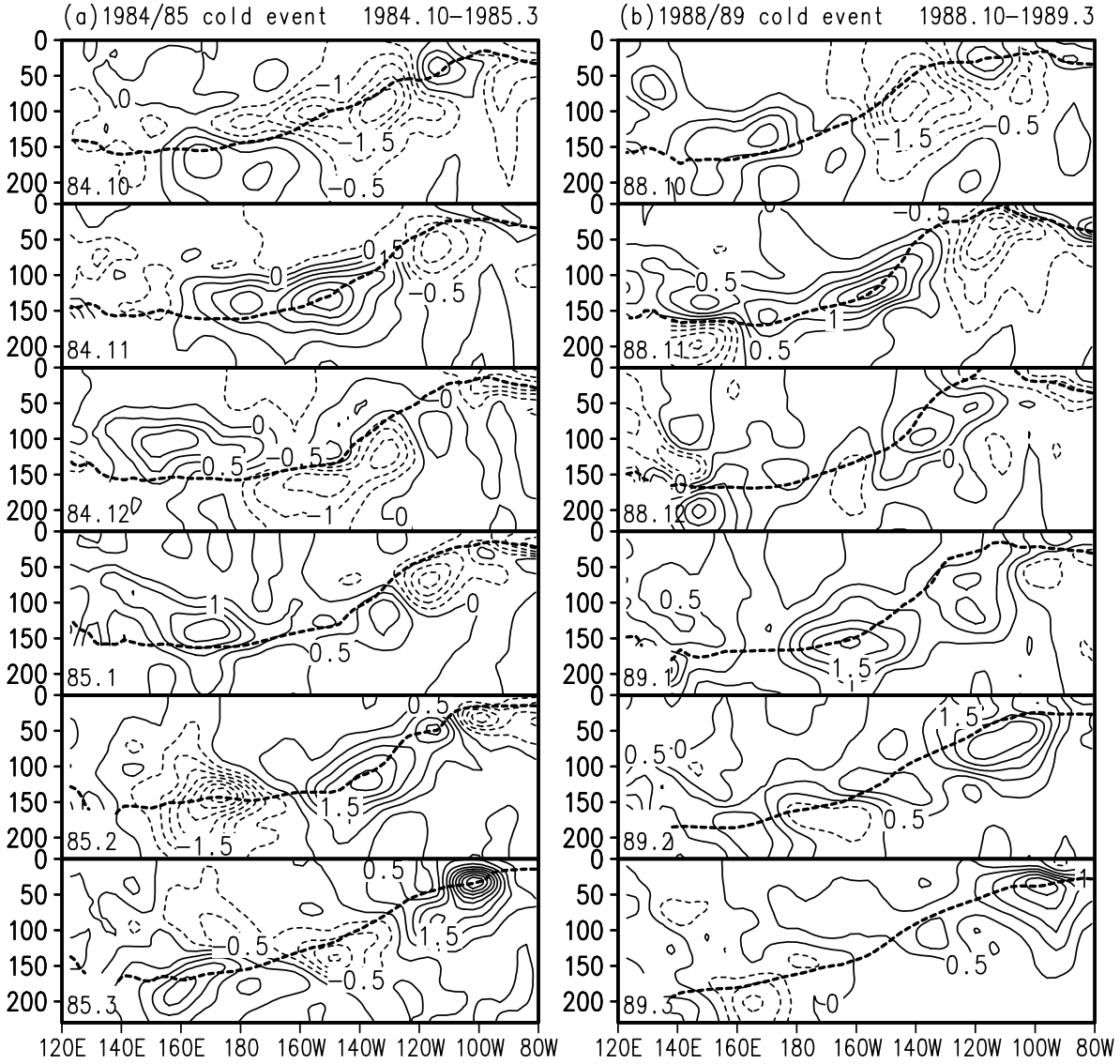
(a)1984/85 cold event 1984.10–1985.3
(b)1988/89 cold event 1988.10–1989.3
84.10
84.11
84.12
85.1
85.2
85.3
88.10
88.11
88.12
89.1
89.2
89.3
0
50
100
150
200
120E 140E 160E 180 160W 140W 120W 100W 80W

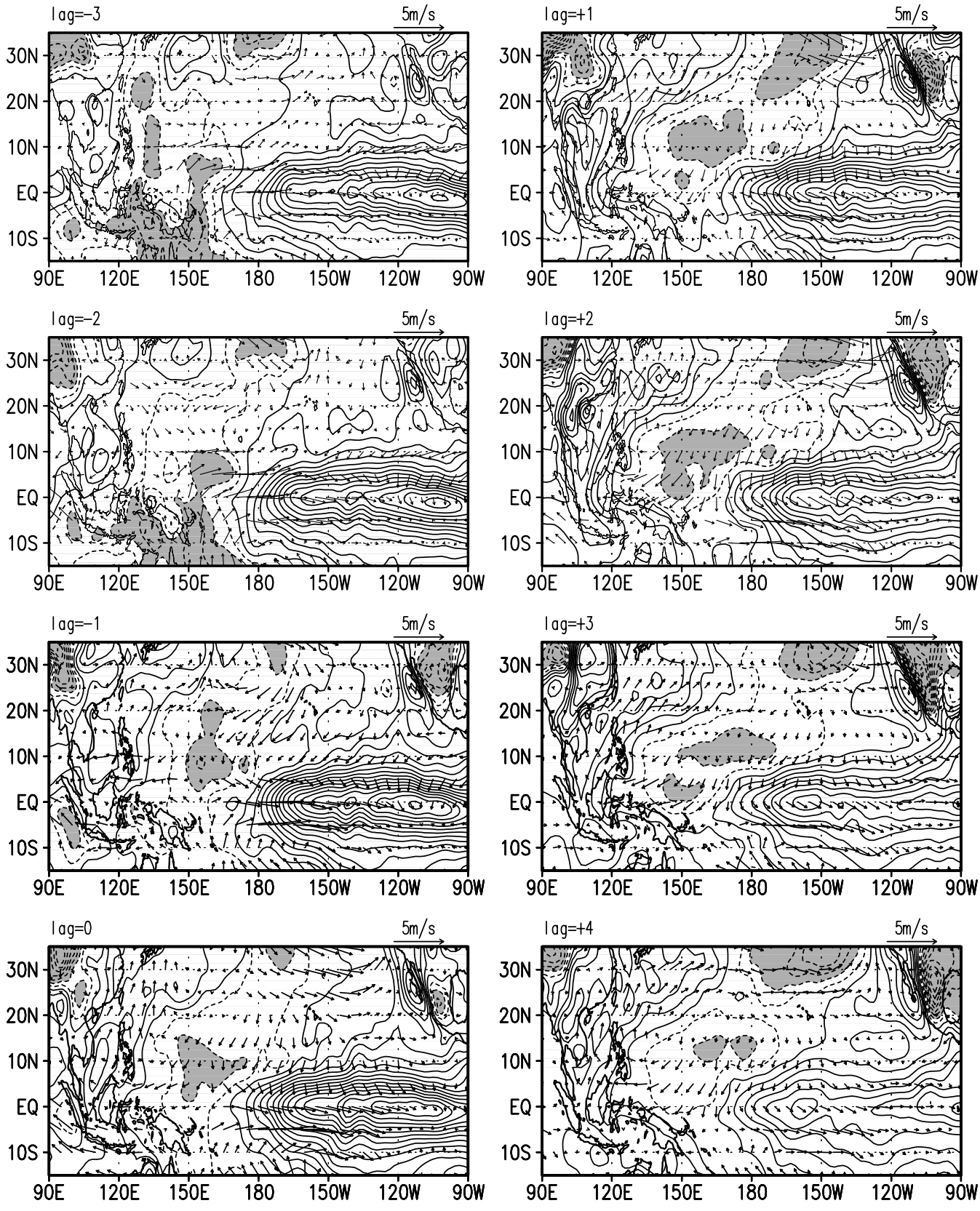
lag=-3
5m/s
lag=+1
5m/s
lag=-2
5m/s
lag=+2
5m/s
lag=-1
5m/s
lag=+3
5m/s
lag=0
5m/s
lag=+4
5m/s
30N
20N
10N
EQ
10S
90E
120E
150E
180
150W
120W
90W

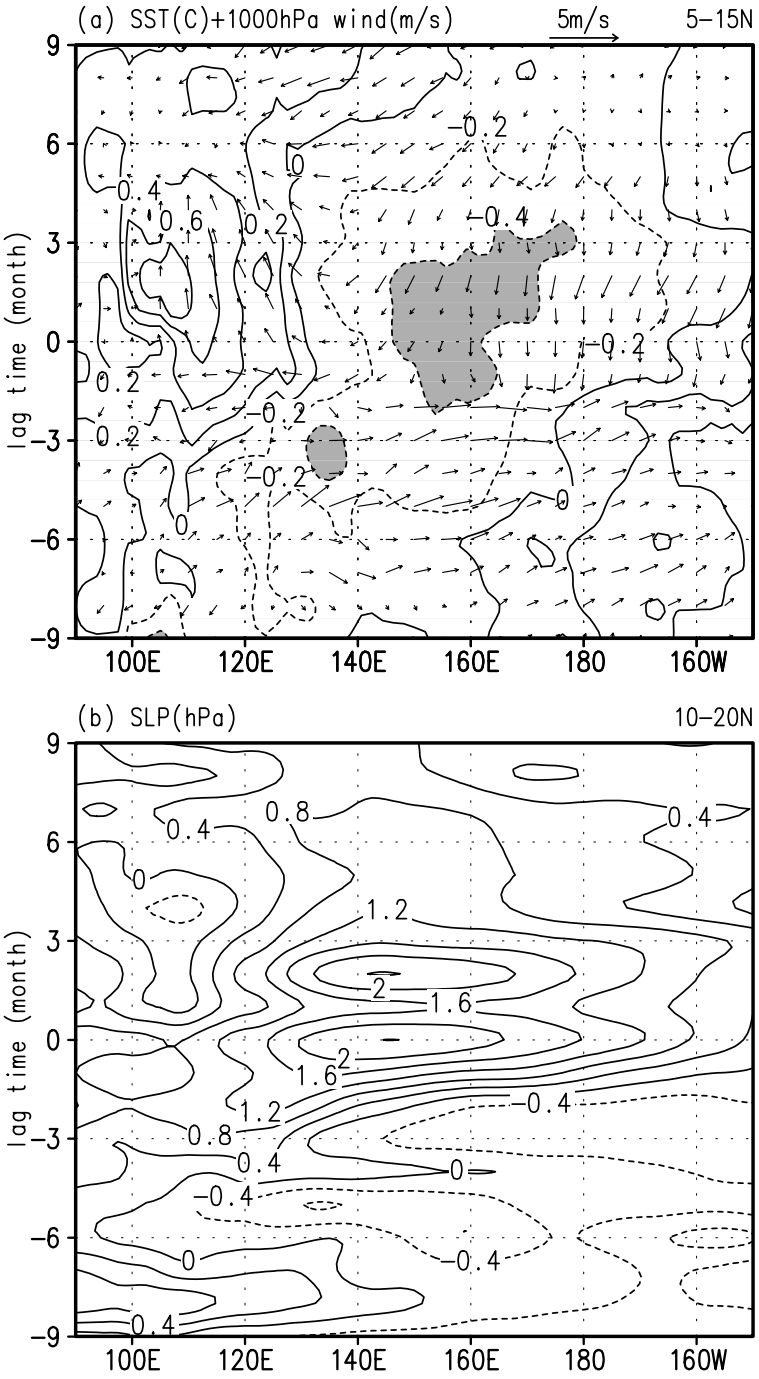
(a) SST(C)+1000hPa wind(m/s)
5m/s
5-15N
lag time (month)
9
6
3
0
-3
-6
-9
100E
120E
140E
160E
180
160W
0.4
0.6
0.2
0
-0.2
-0.4
(b) SLP(hPa)
10-20N
0.8
1.2
2
1.6

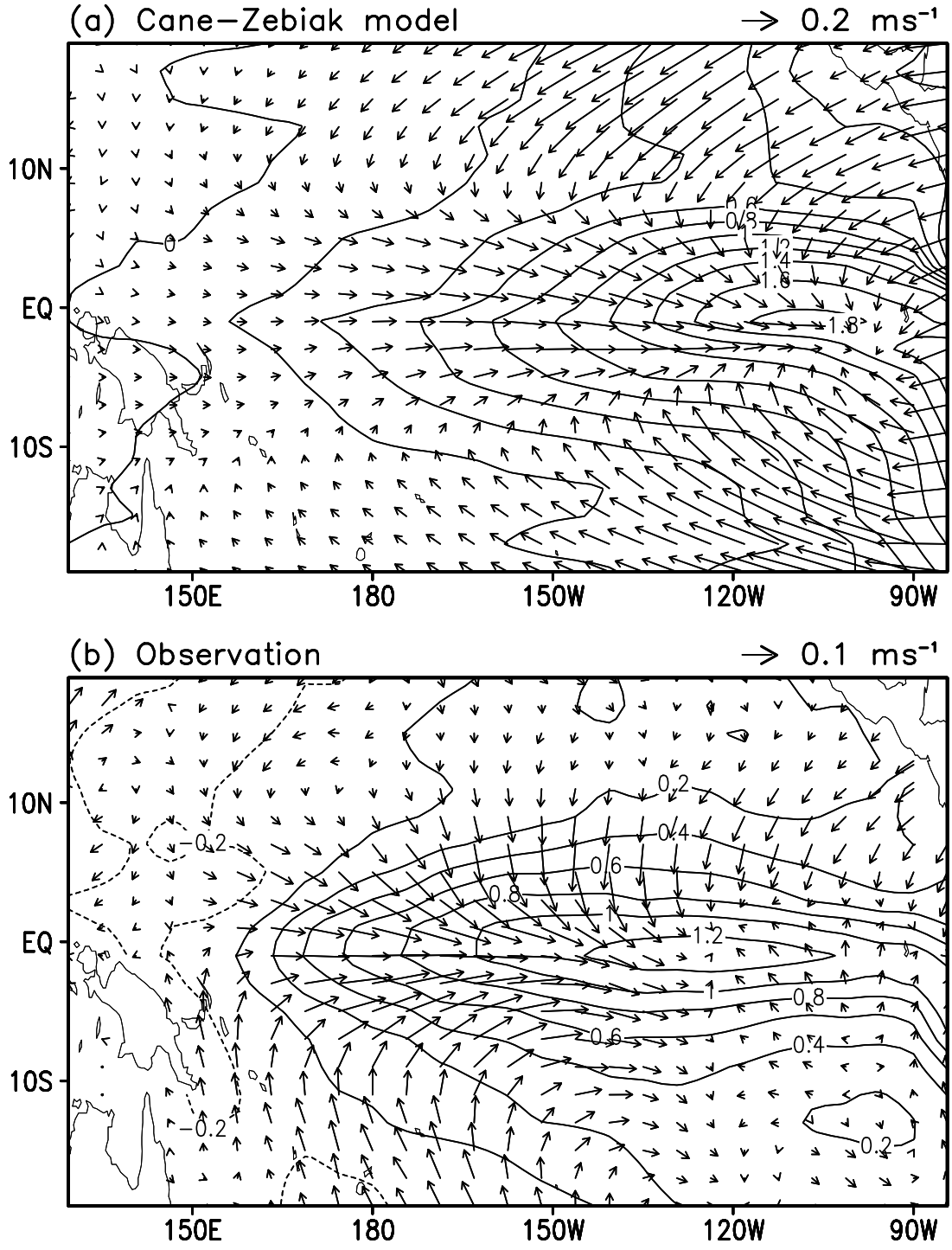
(a) Cane−Zebiak model
→ 0.2 ms⁻¹
10N
EQ
10S
150E
180
150W
120W
90W
0
0.2
0.4
0.6
0.8
1
1.2
1.4
1.6
1.8
(b) Observation
→ 0.1 ms⁻¹
10N
EQ
10S
150E
180
150W
120W
90W
−0.2
0.2
0.4
0.6
0.8
1
1.2
0

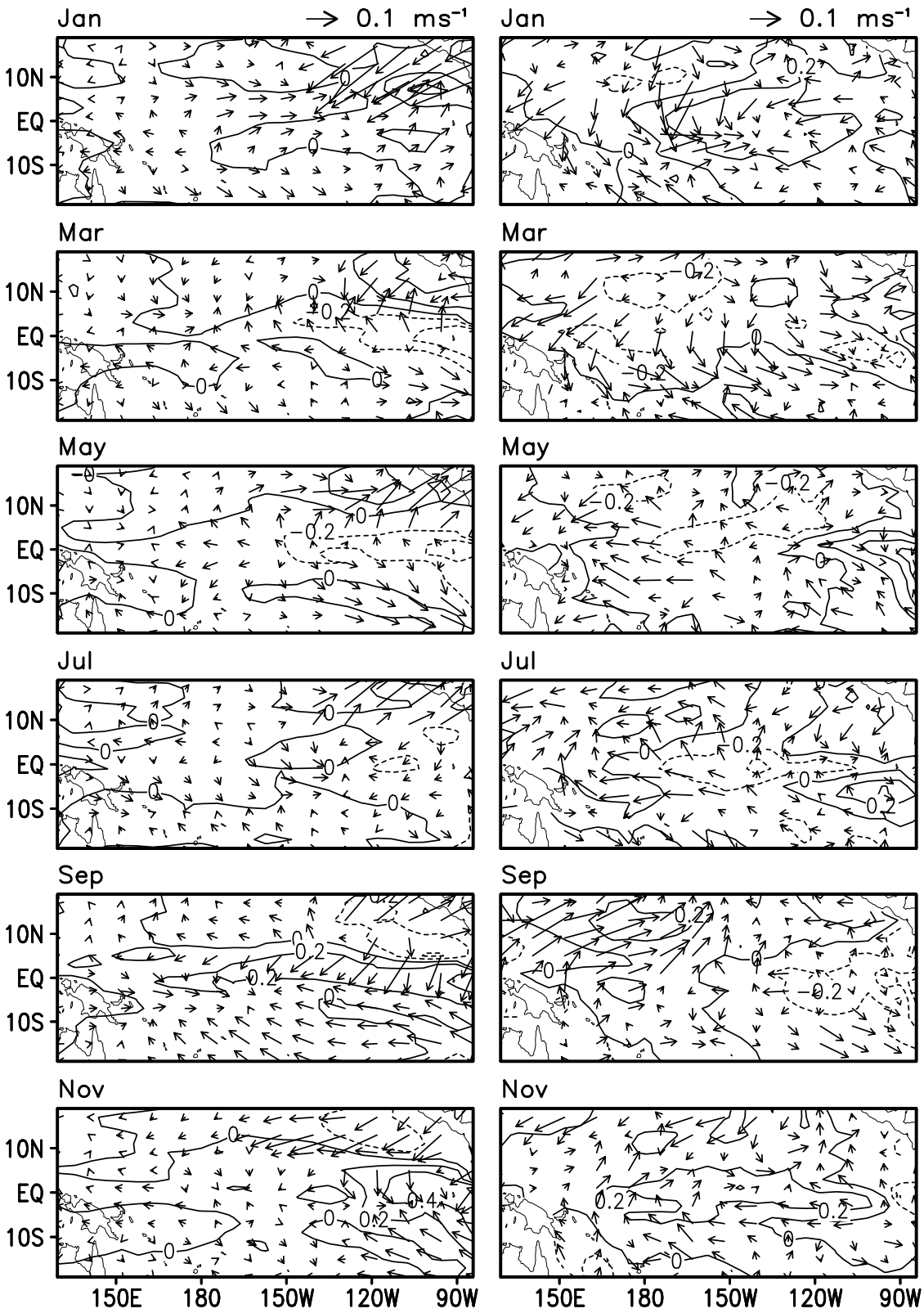
(a) CZ MODEL
(b) OBSERVATION
Jan
→ 0.1 ms⁻¹
Mar
May
Jul
Sep
Nov
10N
EQ
10S
150E
180
150W
120W
90W

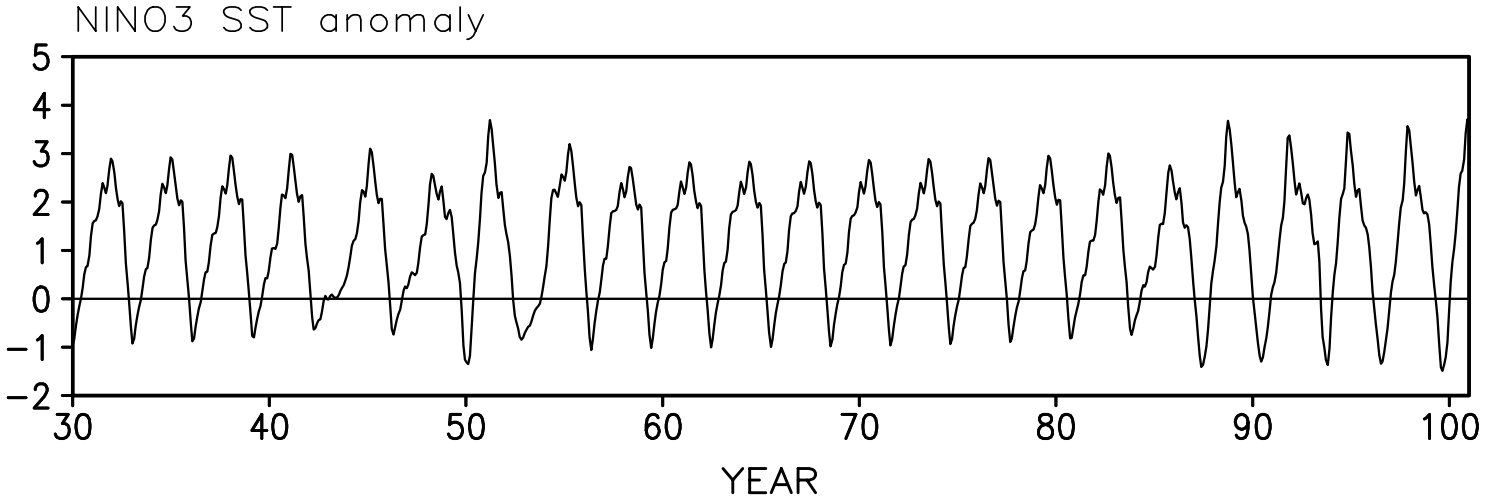
NINO3 SST anomaly
5
4
3
2
1
0
−1
−2
30
40
50
60
70
80
90
100
YEAR

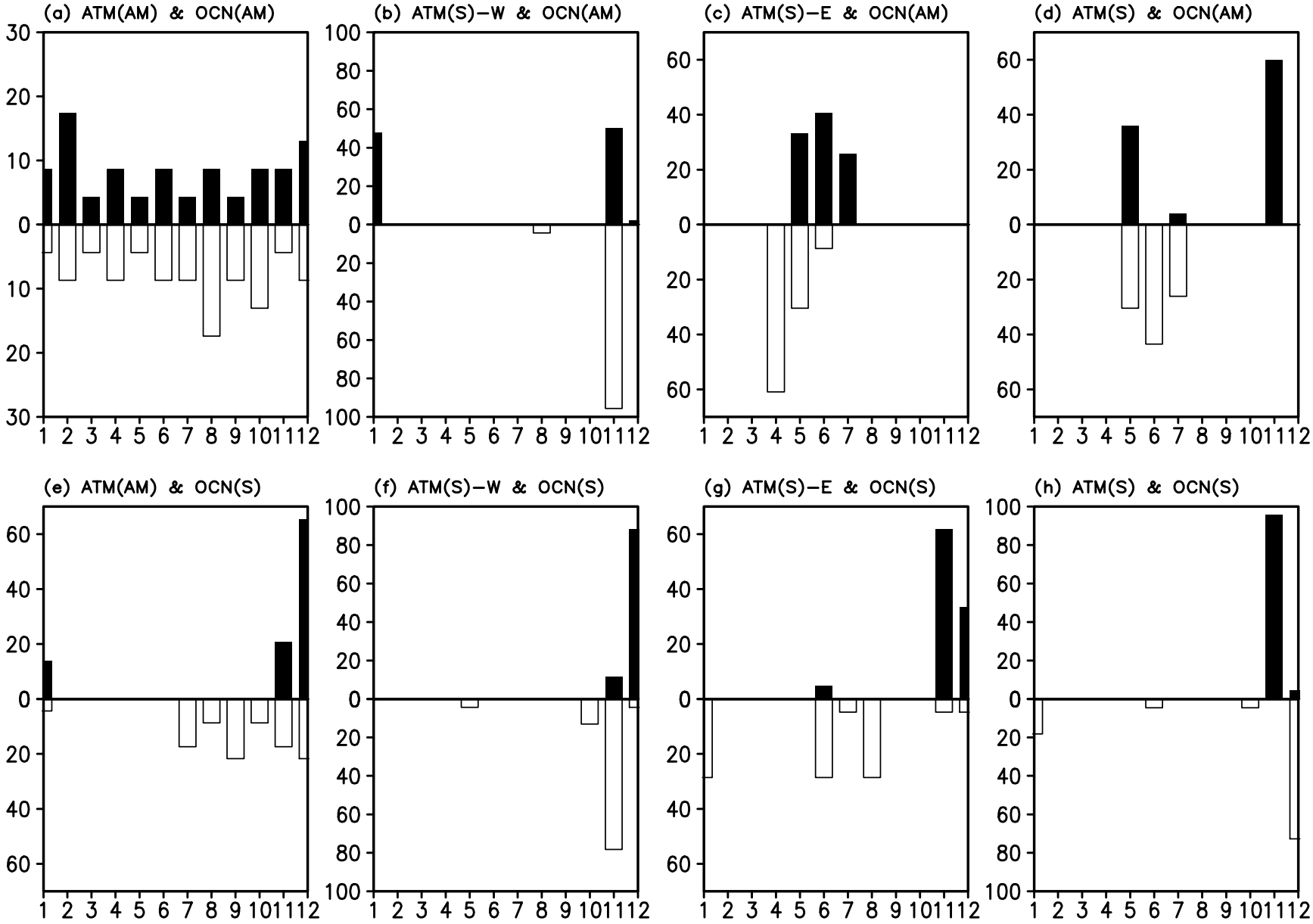
(a) ATM(AM) & OCN(AM)
(b) ATM(S)−W & OCN(AM)
(c) ATM(S)−E & OCN(AM)
(d) ATM(S) & OCN(AM)
(e) ATM(AM) & OCN(S)
(f) ATM(S)−W & OCN(S)
(g) ATM(S)−E & OCN(S)
(h) ATM(S) & OCN(S)

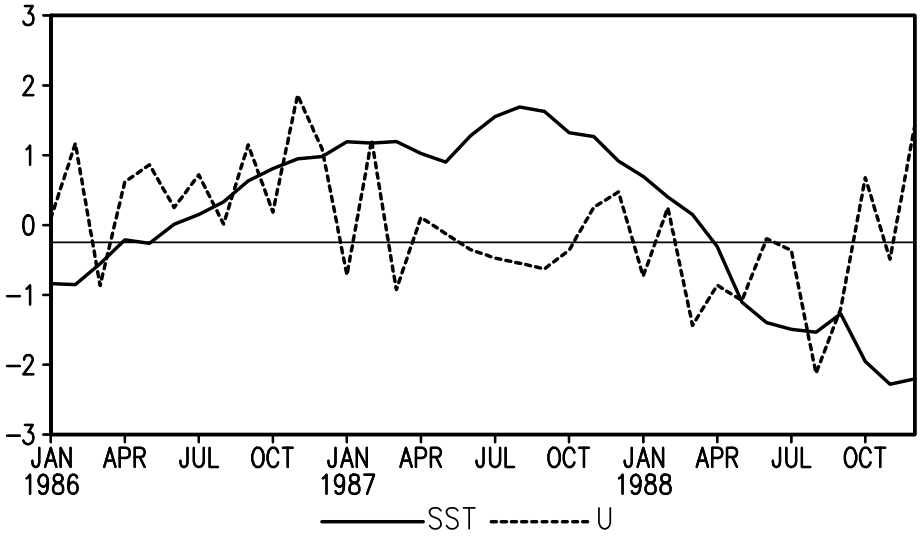
3
2
1
0
−1
−2
−3
JAN
1986
APR
JUL
OCT
JAN
1987
APR
JUL
OCT
JAN
1988
APR
JUL
OCT
SST
U